iScience

CellPress
OPEN ACCESS

Article

NSC48160 targets AMPKα to ameliorate nonalcoholic steatohepatitis by inhibiting lipogenesis and mitochondrial oxidative stress

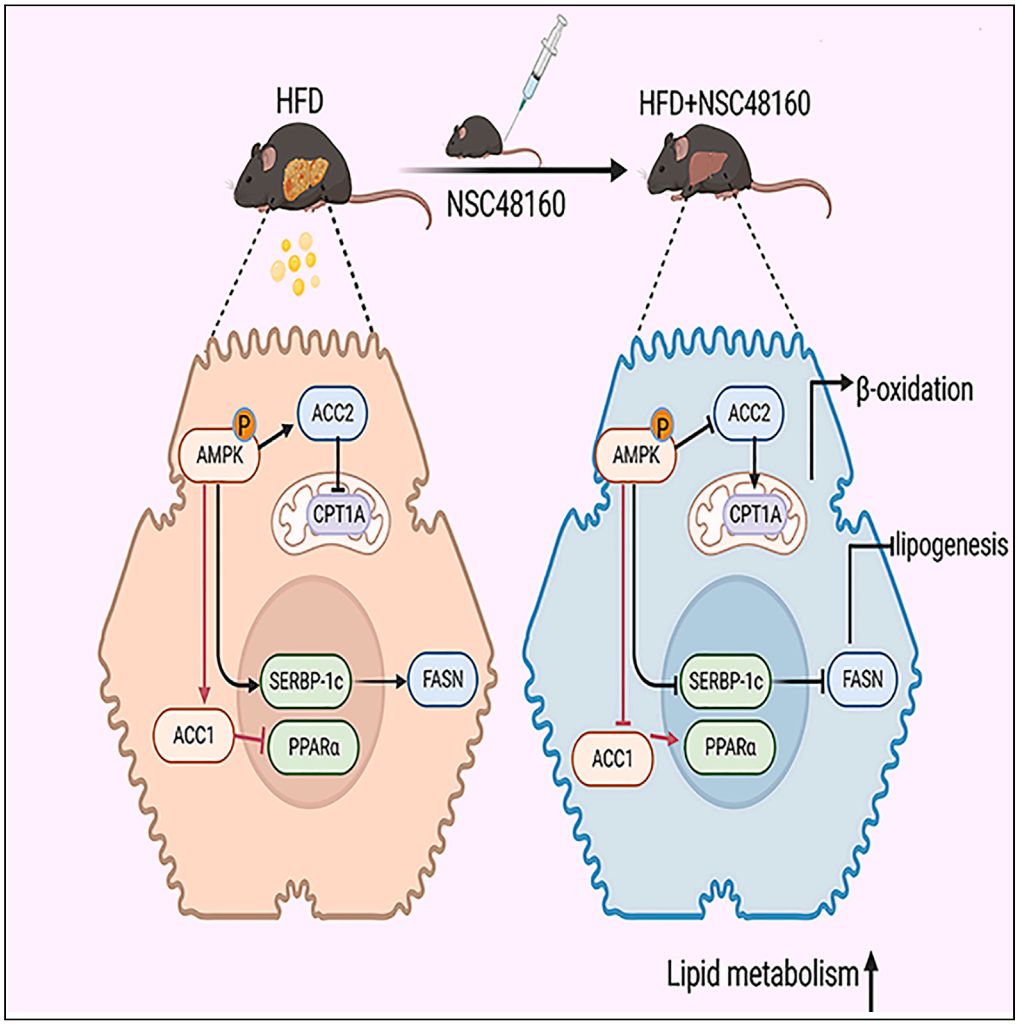

Jiaxin Zhang, Zuojia Liu, Xunzhe Yin, Erkang Wang, Jin Wang

zjliu@ciac.ac.cn (Z.L.)
jin.wang.1@stonybrook.edu (J.W.)

Highlights

Nonalcoholic fatty liver disease is associated with metabolic disorder

NSC48160 regulates hepatic lipid metabolism in fatty acid oxidation and lipogenesis

NSC48160 decreased inflammation and impaired mitochondrial function by targeting AMPK

NSC48160 is a promising agent against nonalcoholic steatohepatitis

Zhang et al., iScience 27, 108614
January 19, 2024
https://doi.org/10.1016/j.isci.2023.108614

iScience

CellPress
OPEN ACCESS

Article

NSC48160 targets AMPKα to ameliorate nonalcoholic steatohepatitis by inhibiting lipogenesis and mitochondrial oxidative stress

Jiaxin Zhang,[1,2] Zuojia Liu,[1,4,*] Xunzhe Yin,[1] Erkang Wang,[1,2] and Jin Wang[3,*]

SUMMARY

Hepatic steatosis, which is triggered by dysregulation of lipid metabolism and redox equilibrium in the liver, is regarded as a risk factor in the non-alcoholic fatty liver disease (NAFLD). However, pharmacologic engagement of this process is difficult. We identified the small molecule NSC48160 as an effective agent against nonalcoholic steatohepatitis (NASH). We found that NSC48160 significantly lowered hepatic lipid levels *in vitro* and *in vivo* by activating the AMPKα-dependent pathway. AMPKα regulated its downstream pathway involved in lipogenesis (SREBP-1c/FASN pathway) and fatty acid oxidation (PPARα pathway). Metabonomics analysis combined with RNA-sequencing profiling revealed that NSC48160-induced lipogenesis is modulated by lipid metabolism. Moreover, NSC48160 dramatically reduces reactive oxygen species (ROS) production, restores the levels of the membrane potential and NAD^+/NADH ratio, and improves mitochondrial respiration. These findings suggest that NSC48160 is a promising hit compound in the pursuit of a pharmacological approach in the treatment of NASH.

INTRODUCTION

Nonalcoholic fatty liver disease (NAFLD), also known as metabolic dysfunction-associated fatty liver disease, is characterized by deposited lipid droplets and impaired lipid metabolism in the liver.[1] NAFLD is a wide spectrum of liver diseases ranging from simple steatosis to nonalcoholic steatohepatitis (NASH), which further progresses to cirrhosis or even more advanced disease stages.[2,3]Thus, it is urgent to develop therapeutic targets and pharmaceutical therapies to delay or terminate the progression of NASH to lower the expanding health care burden worldwide. Multiple risk factors have been shown to contribute to the pathogenesis of NASH, such as hepatic lipid droplet accumulation concomitant with free cholesterol accumulation.[4] To date, approved medicines for NASH are scarce because the pathogenesis of NASH and the molecular mechanism underlying the promotion of lipid metabolism in hepatocytes are not well known.[5]

Given that the pathogenesis of NAFLD is a complicated process, an ideal drug target should be a signaling hub factor that controls the pathophysiological pathway. AMPK as a master regulator of metabolic pathways slows down the critical biosynthetic process by phosphorylating its target proteins.[6,7] Metformin and several experimental compounds have been shown to improve NAFLD in preclinical animal models by increasing the activity of AMPK.[8] More recently, we reported that the natural product gallic acid alleviates NASH in NAFLD animal models by directly activating the AMPK-mediated ACC-PPARα pathway via dual regulation of lipid metabolism and mitochondrial function.[9] Therefore, it is conceivable that activating the AMPK signaling axis could be an attractive strategy for NAFLD treatment.[10]

AMPK is directly activated in response to a binding interaction, which attenuates anabolic lipid synthesis and catabolic β-oxidation. This cascade reaction involves multiple branches of AMPK-mediated cellular metabolism, including reductions in ACC,[11] resulting in the weakened conversion of acetyl-CoA to malonyl-CoA (the first committed step in *de novo* lipogenesis). Malonyl-CoA is an inhibitor of carnitinepalmitoyl transferase 1A (CPT1A), which is required for the uptake of fatty acyl-CoA into mitochondria, and thus, a reduction in malonyl-CoA stimulates fatty acid oxidation (FAO) and inhibits lipogenesis.[12] In addition to these short-term effects, activated AMPK inhibits the transcription of lipogenic genes by phosphorylating the transcription factor, sterol regulatory element binding protein-1c (SREBP-1c).[13] SREBP-1c is a key regulator of lipogenesis and plays a role in activating the transcription of genes that produce rate-limiting lipogenic enzymes such as fatty acid synthase (FASN).[14] Although several putative mechanisms have been proposed to account for the inhibition of the lipid metabolism pathway by AMPK in response to stimuli like mTOR and eEF2K,[15,16] relatively few studies have examined how the ACC-CPT1A/SREBP-1c-FASN pathway is controlled by AMPK in NAFLD. Previous studies have revealed that increased lipogenesis and activated SREBP-1c are observed in NAFLD mouse models.[17] It has been demonstrated that abnormal activation of SREBP-1c drives lipogenesis.[18] Thus, suppressing lipogenesis by inhibiting the AMPK-mediated SREBP-1c pathway might be an effective strategy for treating NASH.

[1]State Key Laboratory of Electroanalytical Chemistry, Changchun Institute of Applied Chemistry, Chinese Academy of Sciences, Changchun 130022, China
[2]School of Applied Chemistry and Engineering, University of Science and Technology of China, Hefei 230026, China
[3]Department of Chemistry and Physics, Stony Brook University, Stony Brook, NY 11794-3400, USA
[4]Lead contact
*Correspondence: zjliu@ciac.ac.cn (Z.L.), jin.wang.1@stonybrook.edu (J.W.)
https://doi.org/10.1016/j.isci.2023.108614

In this work, we identified a promising AMPKα-ACC-SREBP-1c axis inhibitor, NSC48160, named 4-*tert*-butyl-2-[(cyclohexylamino) methyl]-6-methylphenol,that prevents the development of NAFLD induced by a high-fat diet (HFD), allowing for direct activation of AMPK *in vitro* and *in vivo*. Moreover, we elucidated the mechanism by which NSC48160 directly targets AMPKα to block the SREBP-1c signaling pathway and evaluated its therapeutic efficacy for treating NASH in NAFLD mouse models. These promising findings suggest that NSC48160 could be a useful therapeutic tool to treat NAFLD.

RESULTS

NSC48160 ameliorates NAFLD in diet-induced mice

NSC48160 has been proven to treat HCC by suppressing *de novo* lipogenesis in our laboratory. Given that elevated lipogenesis is also a common feature of NAFLD, it is possible to use NSC48160 for the treatment of NAFLD. Adult C57BL/6J mice were challenged with an HFD for 16 continuous weeks, and received once-daily administration of the vehicle solution (saline) or NSC48160 (50 or 100 mg/kg/d) intragastrically for 4 weeks. Mice fed an HFD and normal chow (NC) diet was used as controls (Figure 1A). NSC48160 has been observed to be effective and nonhepatotoxic at the dose used. HFD-fed mice exhibited fatty liver and hepatomegaly, and protection from pathological changes and steatosis was observed in mice treated with NSC48160 (Figure 1B). Compared with NC-vehicle mice, the body weight of HFD-vehicle mice was significantly increased, while these increases were alleviated by NSC48160 administration. Consistent with fasting body weight augmentation, the white adipose weight (WWs) and white adipose weight-to-body weight ratio (WW/BW) in NSC48160-treated mice were notably lower than those in the HFD-vehicle group (Figure 1C). In keeping with that, the LWs and LW/BW ratios were dramatically decreased in HFD-NSC48160mice (Figure 1D). Changes in body weight were evident among the four groups (Figure 1E). Administration of NSC48160 eliminated excess fat accumulation in hepatic intracellular vacuoles as evidenced by less ballooning degeneration in the hepatocytes of HFD-NSC48160 mice by hematoxylin and eosin (H&E) and oil red O staining (Figure 1F). HFD-NSC48160 mice also revealed lower levels of plasma triglycerides and were protected from diet-induced elevations in total cholesterol, both HDL-C and LDL-C (Figure 1G). Furthermore, NSC48160 restored the biomarkers of HFD-fed liver injury, as seen in decreased serum ALT and AST activity, which is the biochemical markers of hepatocellular injury (Figure 1H). Interestingly, NSC48160 treatment showed less significant effects on mouse liver characteristics and functions under NC feeding conditions (Figures 1B–1H). Following 16 weeks of NC feeding, mice that received NSC48160 showed minimal effects on the functions and histological characteristics of key organs, as shown by comparable serological index levels and H&E staining images (Figure 1I). In general, our investigation clarifies that NSC48160 is capable of alleviating hepatic steatosis in HFD-fed mice.

NSC48160 reduces lipid accumulation *in vitro*

Since hepatocytes are the primary cell type of the liver and are responsible for fatty acid induced lipotoxicity, we subsequently investigated the direct effects of NSC48160 on hepatocytes under conditions of metabolic stress. HepG2 and BEL-7402 cells were treated with palmitic acid and oleic acid (PO) in the presence of different concentrations of NSC48160 or vehicle solution. To avoid the toxicity caused by PO in this study, a CCK-8 assay was performed to evaluate the maximum nontoxic concentration of OA (0.4 mM) and PA (0.2 mM) (Figure 2A). Similarly, the effective nontoxic concentration of NSC48160 was confirmed by LDH release and CCK8 assays (Figures 2B and 2C). Consistently, NSC48160 did not cause excessive cell injury and thus demonstrated no significant inhibition of cell growth, which was proven in steatosis hepatocytes by colony formation assays (Figure 2D). Oil red O staining showed that NSC48160 notably decreased PO-stimulated cellular lipid droplet accumulation in a dose-dependent manner compared with that of the control group (Figure 2E). Moreover, the contents of intracellular TG and T-CHO in the PO-stimulated cells were significantly suppressed in the NSC48160-treated group (Figure 2F). Hepatocellular death is a common feature of NASH. Improving liver damage caused by hepatocellular death is a major goal of NASH therapy. The apoptotic marker Bax and cleaved-caspase 9 were upregulated by exposure to PO, as shown in Figure 2G, whereas this effect was reversed by NSC48160 treatment. Consistently, immunofluorescence analysis showed that the signals of cleaved-caspase-9 were clearly detected in the PO group. Compared to the PO group, cleaved-caspase-9 was similarly expressed in the two treatment groups in a downward trend (Figure 2H), which strongly suggests that apoptosis is not triggered by NSC48160 under the condition of drug therapy during lipid-accumulation induction. The findings implied that NSC48160 treatment rescued the injury caused by PO by inhibiting caspase-9-mediated apoptosis. Collectively, these results demonstrate that NSC48160 attenuates PO-stimulated lipid accumulation *in vitro* and shields hepatocytes from damage caused by PO.

NSC48160 inhibits the AMPKα-SREBP-1C-FASN signaling pathway

To gain insight into the molecular mechanisms and biological functions by which NSC48160 ameliorates NAFLD, we next analyzed the metabolic pathway from PO-treated hepatocytes and liver samples from HFD-fed mice. The untargeted metabonomics analysis was performed to detect a wide range of metabolites in both the HFD-NSC48160 and HFD-vehicle groups. The OPLS-DA model showed that metabolites in the two groups were clearly separated (Figure 3A). It is clear that there is a significant metabolic change in these NAFLD mice. The permutation test of the model showed that R^2X was 0.336, R^2Y was 0.954, and Q^2 was 0.664($p < 0.005$) (Figure 3B). Kyoto Encyclopedia of Genes and Genomes (KEGG) is a database resource for understanding high-level functions and utilities of the biological system. KEGG pathway enrichment analysis of all differentially abundant metabolites proved that the samples between the two groups were different in the metabolic pathways of cholesterol metabolism, glutathione metabolism and biosynthesis of amino acids involved in lipid metabolism (Figure 3C). Furthermore, the STRING tool was used to assess the functional relations and networks among these proteins. Herein, a protein-protein interaction (PPI)

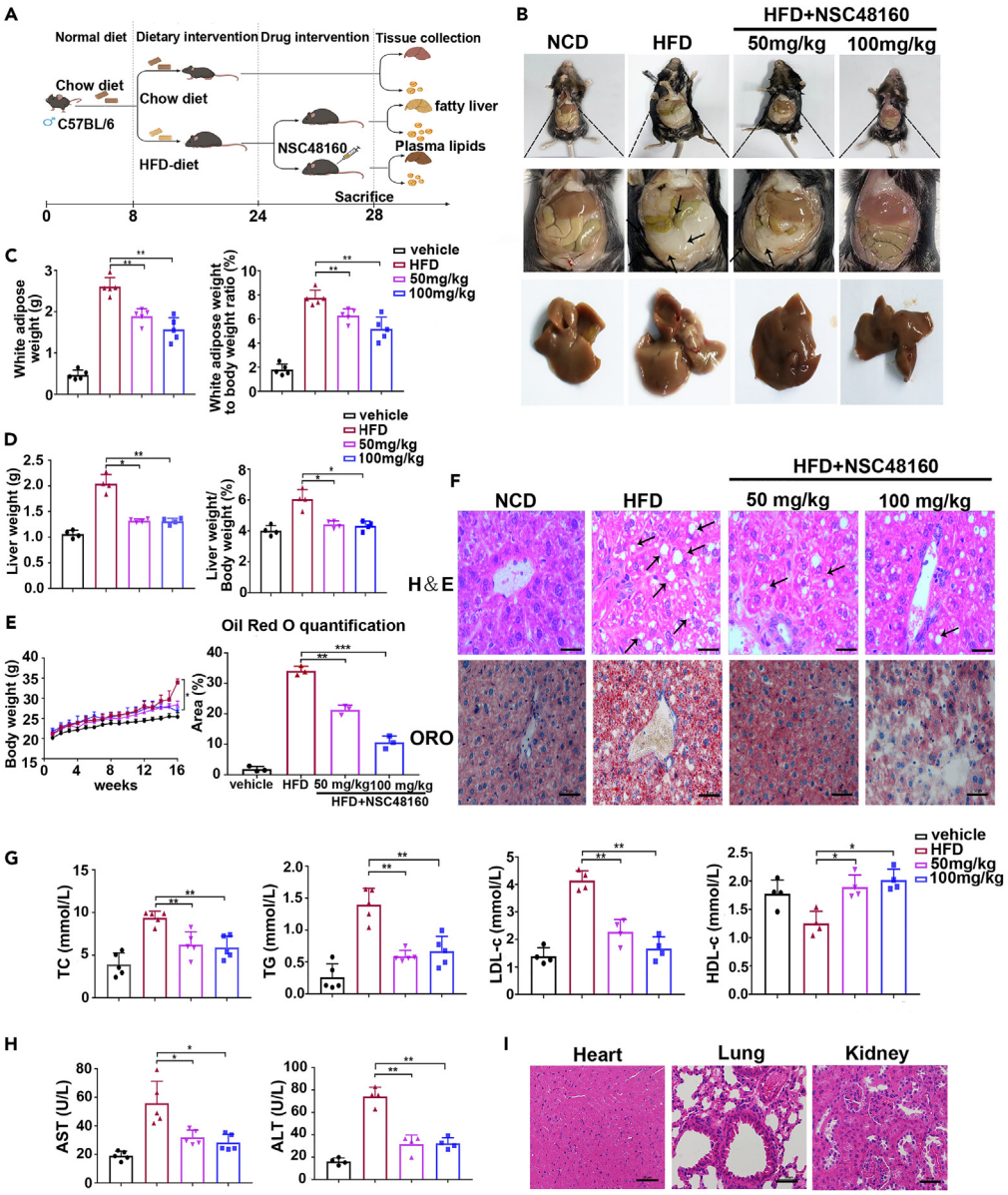

Figure 1. NSC48160 ameliorates HFD-induced hepatic steatosis in mice

(A) Schedule diagram shows the time points of HFD diet supplementation at week 8 for 16 weeks and NSC48160 (100 mg/kg) intraperitoneal injection administration at week 20 for 4 weeks in mice.

(B) Gross anatomical representations of representative adipose tissue and liver from mice in the corresponding groups of mice. Scale bar, 2 cm; n = 8 per group.

(C) White adipose weight and white adipose-to-body weight ratios.

(D) Liver weights and ratios of liver to body weight.

(E) Body weight; n = 4 per group.

(F) H&E and oil red O staining of liver sections from mice in the aforementioned groups. Scale bar, 100 μm. n = 3 per group.

(G and H) Serum lipid content (TG, TC, LDL-C, HDL-C, ALT, and AST) of the indicated mice. n = 5 per group.

(I) Heart, lung, and kidney slices from mice in the aforementioned groups stained with H&E. Scale bar, 100 μm. n = 3 per group. All pooled data presented as the mean ± SEM, *p < 0.05, **p < 0.01, ***p < 0.001.

network is obtained, which comprises DEGs in the lipid metabolism pathway (Figure 3D). AMPKα regulates and coordinates lipid homeostasis in the liver, which is involved in the transcriptional activation of the genes encoding rate-limiting enzymes in lipogenesis, such as FASN, ACC and stearoyl-CoA desaturase1 (SCD1), and fatty acid β-oxidation receives increased attention in relation to the disposal of hepatic FFAs, such as PPARα and CPT1A (Figure 3D). The aforementioned genes were chosen from the hub genes. Accordingly, NSC48160 regulates these

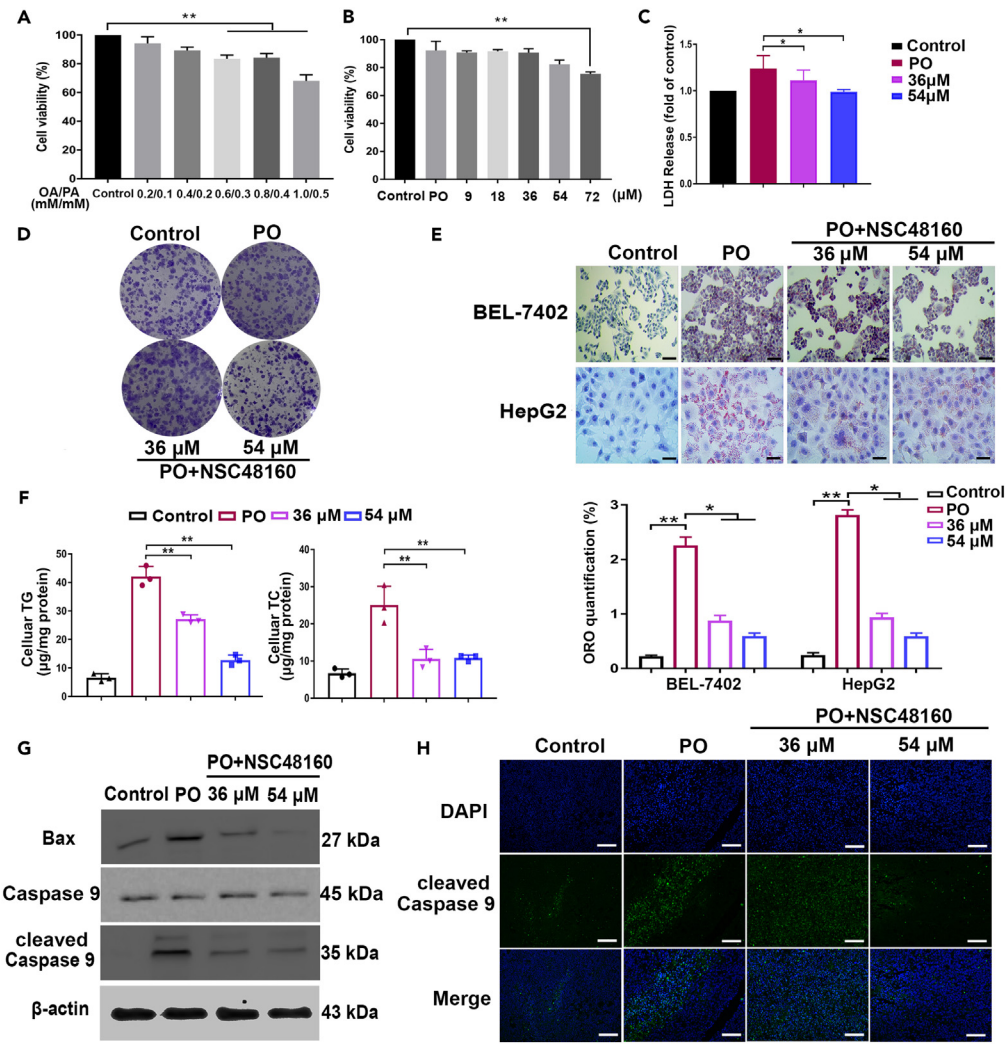

Figure 2. NSC48160 reduces lipid accumulation and promotes lipid metabolism in hepatocytes

(A) The effect of OA/PA on cell viability detected using the CCK-8 assay.

(B) BEL-7402 cells and HepG2 cells were treated with 9, 18, 36, 45, 54, and 72 μM NSC48160 for 24 h. Cell viability was determined by CCK8 assay.

(C) LDH release in each group.

(D) Colony formation of hepatocytes with or without NSC48160 administration with PO.

(E) Representative oil red O staining images of hepatocytes with or without NSC48160 treatment induced with PO for 24 h. Scale bar, 100 μm.

(F) PO increased triglyceride (TG) and total cholesterol (TC) accumulation in HepG2 cells, and treatment with NSC48160 decreased TG and TC accumulation in HepG2 cells.

(G) Western blotting analysis of the key apoptosis markers, Bax and caspase 9. β-actin was used as a loading control.

(H) Representative confocal pictures display caspase 9 labeling alone (green) or in conjunction with nuclear staining using DAPI (blue). n = 3 each group. The data are presented as the mean ± SEM, *p < 0.05, **p < 0.01.

processes through the modulation of the master regulator of lipogenesis and β-oxidation. Among the most lipid metabolism related pathways, AMPK is the most drastically altered upstream regulator in mouse livers and hepatocytes. AMPK activation could counteract these effects via a variety of mechanisms, which can be partly proven by Figure 3E. Experimentally, our results confirmed the increased protein ratios of *p*-AMPK/AMPK and *p*-ACC/ACC, indicating that AMPK activation could promote *p*-ACC but inhibit ACC expression, thus promoting the oxidative metabolism of fatty acids in hepatocytes. Activation of AMPKα in the liver reduced the expression of lipogenic genes, including SREBP-1c and FASN, and the intracellular lipid accumulation while increasing PPARα expression (increasing fatty acid clearance via mitochondrial FAO) *in vitro* and *in vivo* (Figures 3E and 3F). Moreover, immunohistochemistry (IHC) analysis further confirmed the increased protein expression of *p*-AMPK and PPARα in liver sections (Figure 3G). In conclusion, the NSC48160-mediated AMPKα-SREBP-1c-FASN axis results in an inhibitory effect on lipid accumulation *in vitro and in vivo*.

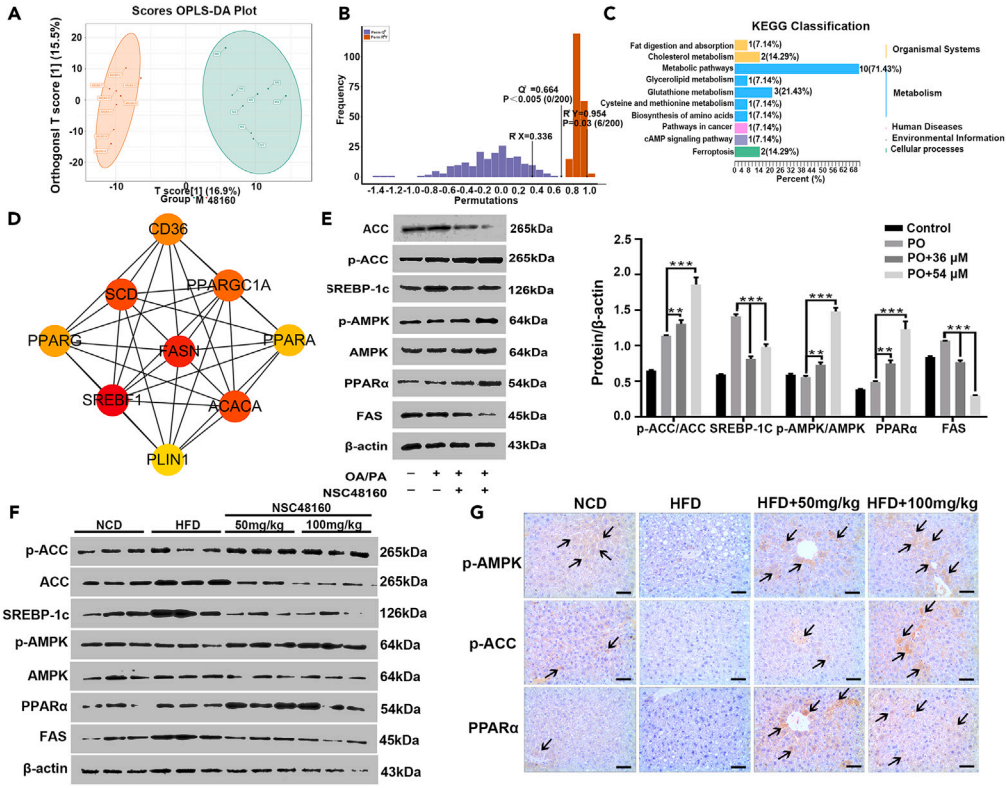

Figure 3. Metabonomics reveals the central target of NSC48160 in HFD-induced mice

(A) OPLS-DA showed the possible discrimination of metabolites in the treatment group and control group (n = 8) as indicated. 48160-1–48160-5: the NSC48160 treatment samples for metabonomics, M1–M5: the HFD-induced mice samples for metabonomics.

(B) R^2 and Q^2 represent goodness of fit and prediction respectively, and the p value shows the significance level of the model (x axis = predictive components, y axis = orthogonal component).

(C) The top 10 pathways in rich factors of the gene pathway enrichment.

(D) Protein-protein interaction (PPI) network of lipid metabolism from metabonomics.

(E) The levels of *p*-ACC, SREBP-1C, *p*-AMPK, PPARα and FASN in hepatocytes were assessed by western blotting. β-actin was used as a loading control, n = 3. Representative blots of three independent experiments are shown.

(F) The levels of *p*-ACC, SREBP-1C, *p*-AMPK, PPARα, and FASN were assessed by western blotting in mice, n = 3.

(G) Immunohistochemical staining of liver sections from the indicated mice. Scale bars, 100 μm, n = 3. All pooled data presented as the mean ± SEM, **p < 0.01, ***p < 0.001.

NSC48160 changes metabolic profiles in mouse liver tissues

To better understand the metabolic mechanism in the NAFLD model, we analyzed the metabolic patterns in liver tissues derived from HFD-vehicle mice and HFD-NSC48160 mice, respectively. The malate-aspartate shuttle is a biochemical system in eukaryotic cells that transports electrons transmitted during glycolysis across the semipermeable mitochondrial intima for oxidative phosphorylation (OXPHOS). Compared with the control group, the liver tissues from HFD-NSC48160 mice showed promotion of OXPHOS, as evidenced by the increased levels of malate and aspartate (Figure 4A). Simultaneously, the TCA cycle was promoted by NSC48160 due to the increasing levels of citrate and oxaloacetate in liver tissues from HFD-NSC48160 mice (Figure 4A). Consistent with these results, the expression of the enzymes involved in glycolysis and the TCA cycle was promoted, as observed for lactate dehydrogenase A (LDH-A), lactate dehydrogenase B (LDH-B), pyruvate dehydrogenase (PDH-β) and pyruvate dehydrogenase kinase 1 (PDK1) (Figure 4B). Additionally, the expression of CPT1A and PPARα was upregulated, and their activities modestly increased (Figure 4C), indicating enhanced FAO. Furthermore, the urea cycle in humans, located exclusively in the liver, has evolved to remove ammonia. The enzymes involved in this process are carbamoyl phosphate synthetase 1 (CPS1) and the key rate-limiting enzymeargininesuccinatesynthetase1 (ASS1). Many lines of study have indicated that mitochondrial dysfunction can occur in NAFLD. It is conceivable that mitochondrial injury alters the CPS1 and ASS1 genes, leading to reduced expression and function. However, their high expression in the liver tissue from the HFD-NSC48160 mice revealed an improved urea cycle and alleviated hyperammonemia and liver damage (Figure 4D). As seen intuitively in a network built, metabolites associated with the citric acid cycle and FAO are positively correlated, indicating a potential role in enhancing lipid metabolism (Figure 4E). Based on these metabolic traits of hepatocytes, it can be concluded clearly that the addition of NSC48160 in the context of NAFLD mainly promotes lipid metabolism in HFD-challenged liver tissues.

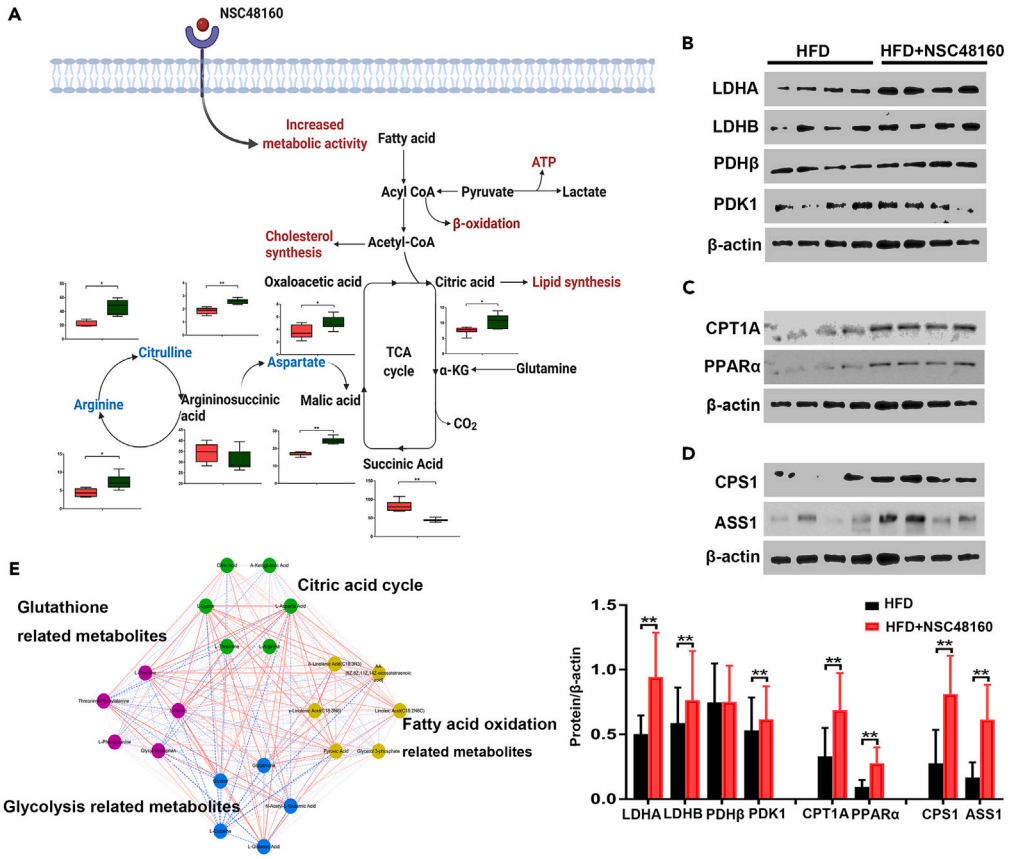

Figure 4. Metabolic profiles in the liver tissue from HFD-induced mice with or without NSC48160

(A) Metabolic changes during oxidative phosphorylation and the TCA cycle in the treatment group compared with the normal group, n = 8.

(B–D) Expression of proteins in glycolysis (LDHA and LDHB), oxidative phosphorylation (PDHβ and PDK1), FAO (PPARα and CPT1A), and the urea cycle (ASS1 and CPS1) in the treatment group liver samples compared with the HFD-induced group liver samples, n = 3.

(E) Correlation network of those significant ($p < 0.05$) related nodes. Colors of nodes represent their categories. All pooled data presented as the mean ± SEM, *$p < 0.05$, **$p < 0.01$.

NSC48160 lowers hepatic lipogenesis-induced oxidative stress and mitochondrial dysfunction

Since increased oxidative stress and mitochondrial dysfunction are two pathological inducing factors of NAFLD, we performed KEGG pathway enrichment to analyze whether these two motivators have potential functional implications in differentially abundant metabolites between the HFD-vehicle and HFD-NSC48160 groups (Figure 5A). Two relatively top-ranked pathways that are highly correlated with liver function are highlighted in 20 metabolic pathways enriched, including glutathione metabolism as well as taurine and hypotaurine metabolism. As shown in Figures 5B and 5C, the symbolic amino acids involved in the synthesis and catabolism of glutathione, such as glutamate, cysteine, glycine, homocysteine and glutamate, are disclosed in the two metabolic pathways closely related to liver function. In contrast, cysterine, cystathionine, and taurine were decreased in the HFD-vehicle group but the addition of NSC48160 reversed these effects. The pharmacological approach to counteract the oxidative stress related to NAFLD progression to NASH, consists of NSC48160 administration, which has been shown to restore GSH levels in hepatocytes (Figure 5C). Intuitively, NSC48160 increases the amount of GSH, which is necessary for reducing the buildup of the incomplete byproducts of FAO. GSH plays a variety of roles in cell physiology, including directly scavenging reactive oxygen species (ROS), such as mitochondrial ROS (mtROS) and cytoplasmic ROS (cROS), which may be identified using specific fluorescent dyes MitoSOX and DCFH-DA, respectively. As indicated in Figure 5D, mtROS and cROS were significantly increased in PO-treated hepatocytes; however, ROS were weakened when NSC48160 was added to PO-treated hepatocytes. NAD^+ is a key coenzyme in redox reactions and is essential for many biological processes, including metabolism, aging and cell death.[19] Increased intracellular ROS levels are the result of decreased NAD^+ levels' effects on ROS. Afterward, the NAD^+ level required for mitochondrial FAO was markedly increased in challenged NSC48160 hepatocytes at a concentration of 54 μM (Figure 5E). The augmentation of NAD^+ levels in the NSC48160-treated hepatocytes directly led to recovery of the NADH-dependent OXPHOS process, which was further supported by the fact that the reduced membrane potential due to the addition of PO gradually returned to the normal level of the control group (Figure 5F). According to these findings, it can be concluded that NSC48160 eases the burden of oxidative stress and mitochondrial dysfunction via a three-step strategy that includes (1) increasing mitochondrial FAO in the steatotic cells, (2) reducing mtROS and cROS from hepatocytes in NAFLD, and (3) enhancing the production of GSH in the steatotic cells (Figure 5G).

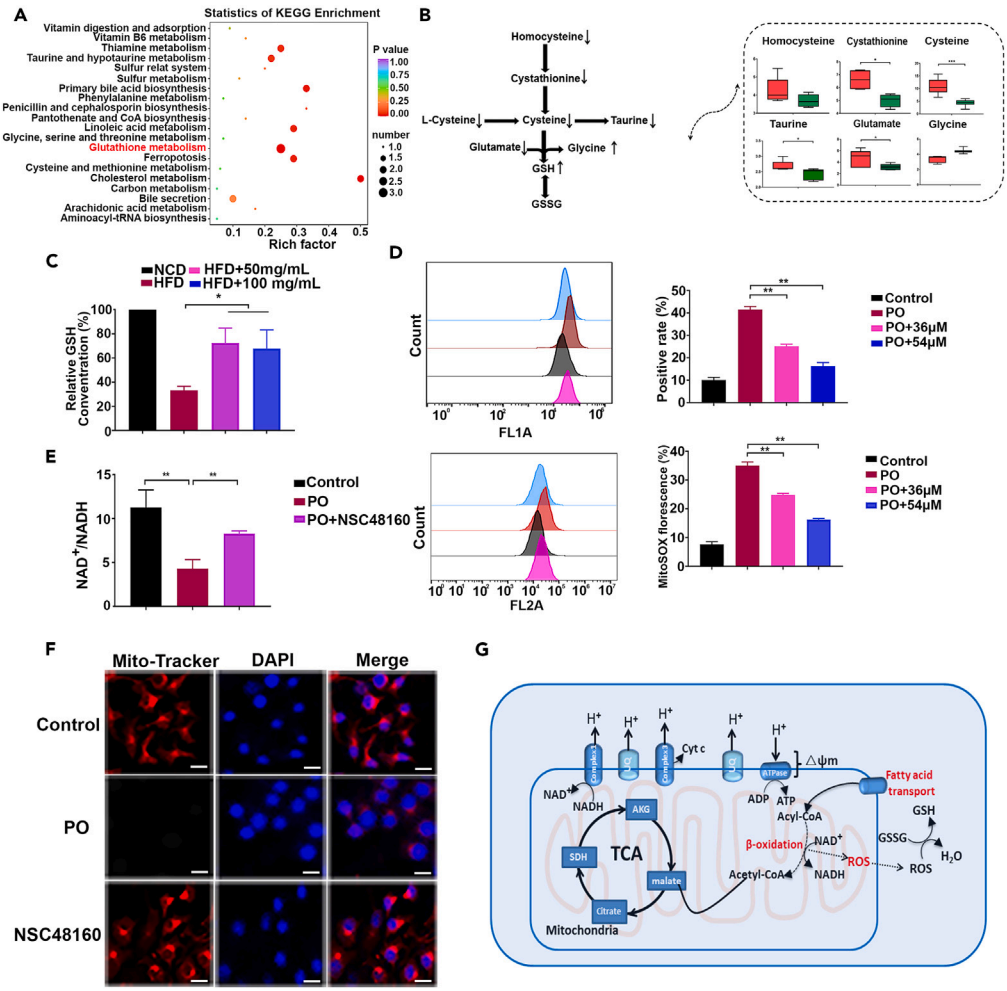

Figure 5. NSC48160 improves the levels of GSH and mitochondrial membrane potential and reduces ROS levels in hepatocytes

(A) The top 20 pathways in rich factors of gene pathway enrichment. The rich factor indicates the ratio of the number of differentially enriched genes to the number of annotated genes in this pathway, and the number indicates the number of genes enriched in this pathway.

(B) Schematic representation of the GSH pathway change from metabonomics. Homocysteine, cystathionine, cysteine, taurine, glutamate, and glycine levels in the HFD and HFD-NSC48160 groups from metabonomics, n = 8.

(C) Intracellular GSH levels of HepG2 cells treated with DMSO, PO, and PO + NSC48160 (n = 3, **p < 0.01).

(D) Flow cytometric analysis of intracellular ROS (up) and mitochondrial ROS (down) levels in HepG2 cells treated with DMSO, PO, and PO + NSC48160 (n = 3, **p < 0.01).

(E) Intracellular NAD^+ and NADH in HepG2 cells treated with DMSO, PO, and PO + NSC48160 (n = 3, **p < 0.01). Scale bars, 50 μm.

(F) Mitochondrial membrane potential change in HepG2 cells induced by PO, together with DMSO and NSC48160 (n = 3).

(G) Molecular mechanisms of the relationship among NAD^+/NADH, ROS, and GSH in hepatocytes. All pooled data presented as the mean ± SEM.

NSC48160 attenuates hepatic lipid accumulation and promotes lipid metabolism via an AMPK-dependent pathway

To determine whether it truly decreases fat deposition through the AMPKα pathway, we tested NSC48160 for the crucial requirement of AMPKα inhibition by knocking down of AMPKα (Figure 6A). NSC48160 reduced lipid formation in PO-induced hepatocytes as anticipated, and this effect was reversed by AMPKα-knockdown (Figure 6B). The reverse effect is seen uniformly in the contents of TG and TC (Figure 6C). To clarify whether the activation of AMPKα is derived from the direct interaction between NSC48160 and AMPKα targets, the possible binding interaction of NSC48160 with AMPK was predicted using molecular docking analysis. The three-dimensional interaction map suggests that NSC48160 and AMPKα may interact directly in the α1β1 domain (Figure 6D). CETSA (cellular thermal shift assay) indicated that NSC48160 has an effect on the protein's thermal stability, implying that there is a direct interaction between NSC48160 and AMPKα within cells *in vivo* (Figure 6E). As shown in Figure 6F, the *in vitro* SPR (surface plasmon resonance) assay showed a strong affinity between NSC48160 and the recombinant AMPKα protein as evidenced by the binding association constant of KD (7.17×10^{-5}M). AMPKα

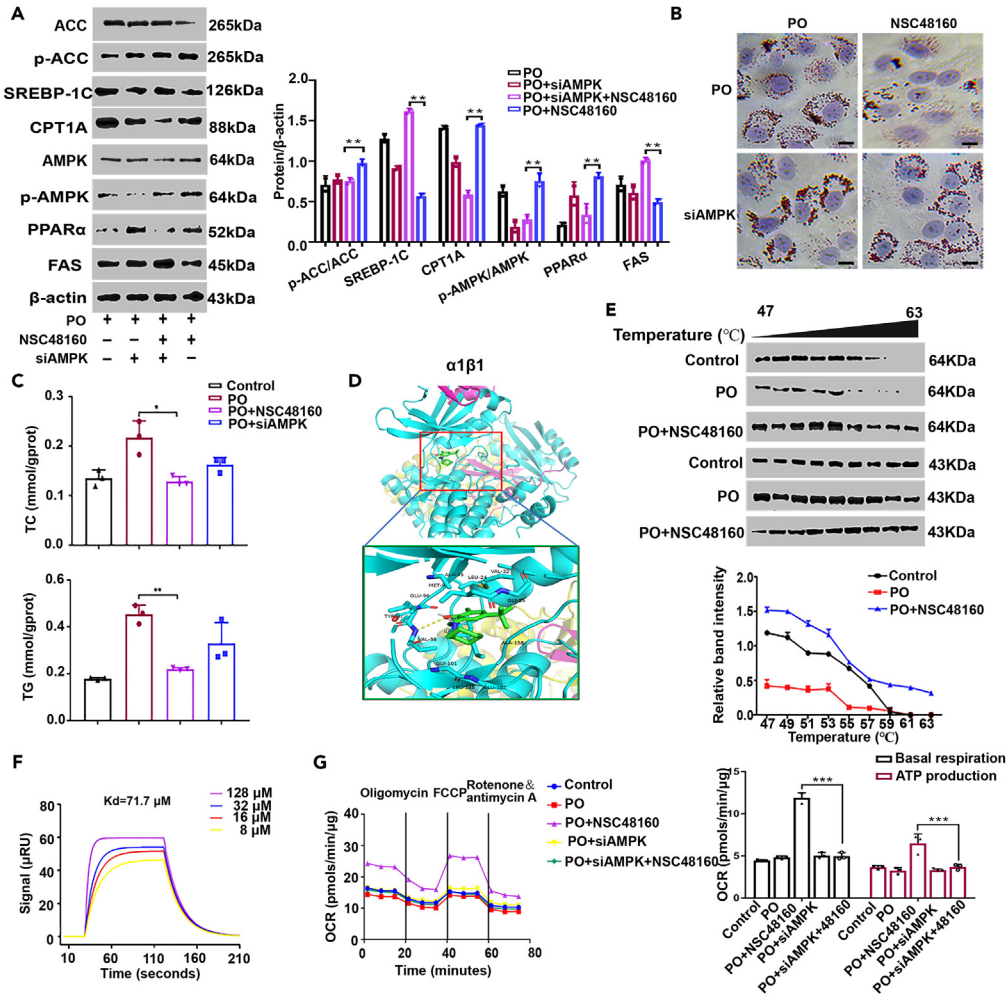

Figure 6. Inhibition of the AMPK pathway abolishes the protective effect of NSC48160 on NAFLD

(A) Immunoblotting analyses of phosphorylated AMPK, ACC, CPT1A, PPARα, and FASN in hepatocytes stimulated by PO with the indicated concentrations of NSC48160, n = 3.

(B) Oil red O staining of the indicated groups.n = 3 replicates. Scale bar, 100 μm.

(C) TG and TC contents of hepatocytes stimulated by PO, together with DMSO or NSC48160. n = 3 replicates.

(D) The binding modes of NSC48160 for the α1β1 AMPK isoform. The α subunit is shown in the illustration and colored cyan and the β subunit was shown in the illustration and colored pink.

(E) CETSA was used to evaluate the binding between NSC48160 and AMPK at the thermodynamic level. The expression of AMPK was detected by western blotting.

(F) The interaction between NSC48160 and recombinant AMPKα protein was analyzed by surface plasmon resonance (SPR) assay.

(G) Mitochondrial respiration of HepG2 cells induced by PO, together with CC and NSC48160. Data represent the mean ± SEM. n = 3, *p < 0.05, **p < 0.01.

behaves as an NSC48160 receptor with a somewhat high affinity for NSC48160, stimulating mitochondrial respiration via the AMPKα/ACC/PPARα pathway. NSC48160 induced an increase in basal respiration and ATP production in HepG2cells, but AMPKα-knockdown obviously reversed this trend (Figure 6G). In summary, these results prove that NSC48160 inhibits steatohepatitis chiefly by targeting AMPKα and regulating downstream pathways.

NSC48160 suppresses fatty acid synthesis and the inflammatory response of hepatocytes *in vitro*

To comprehensively examine the effects of NSC48160 on lipid metabolism and inflammation in hepatocytes under metabolic stress, we used RNA-sequencing (RNA-seq) analysis of HepG2 cells treated with NSC48160 and DMSO control. A heatmap based on the KEGG results revealed that genes related to lipid metabolism were dramatically upregulated by NSC48160 treatment in PO-treated hepatocytes (Figure 7A). A circular enrichment map based on the GO results revealed that lipid metabolic processes (such as lipid storage and fatty acid transport

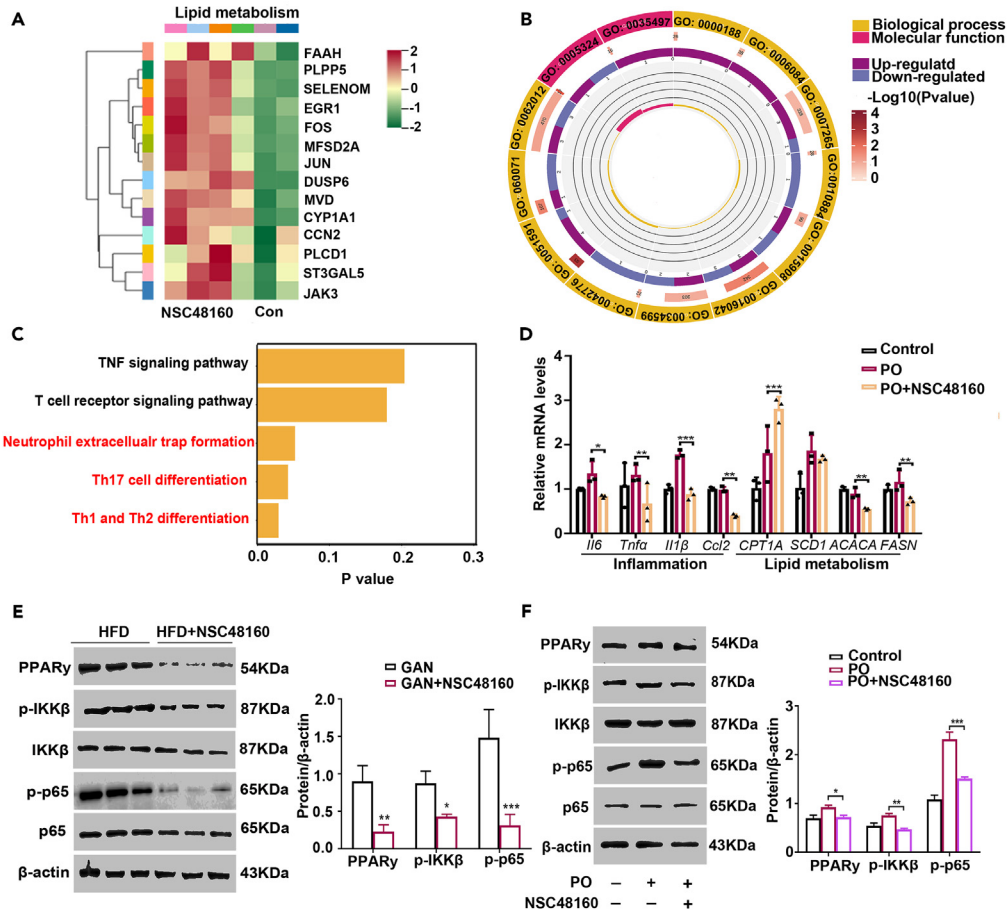

Figure 7. NSC48160promotes lipid metabolism and reduces the inflammatory response in hepatocytes

(A) Heatmap showing the expression pattern of genes related to lipid metabolism in the indicated groups, n = 3.

(B) Circular enrichment map based on GO results for lipid metabolic processes.GO:0000188, inactivation of MAPK activity; GO:0010884, positive regulation of lipid storage; GO:0034599, cellular response to oxidative stress; GO:0051591, response to cAMP; GO:0016042, lipid catabolic process; GO:0007265, Ras protein signal transduction; GO:0006084, acetyl-CoA metabolic process; GO:0060071, Wnt signaling pathway, planar cell polarity pathway; GO:0042776, mitochondrial ATP synthesis coupled proton transport; GO:0015908,fatty acid transport; GO:0062012, regulation of small molecule metabolic process; GO:0005324, long-chain fatty acid transporter activity; GO:0035497, cAMP response element binding.

(C) KEGG pathway enrichment results show inflammation-related pathways.

(D) Expression of genes related to inflammation and lipid metabolism (β-oxidation) in hepatocytes from the indicated groups, n = 3.

(E and F) Western blot analysis of total and phosphorylated IKKβ, p65, and PPARγ in the livers of the indicated mice (left) and hepatocytes (right). β-actin served as a loading control. n = 3 per group. All pooled data presented as the mean ± SEM, *p < 0.05, **p < 0.01, ***p < 0.001.

pathways) were upregulated by NSC48160 (Figure 7B). Chronic inflammation is essential for the deterioration of NAFLD. Therefore, we examined at how NSC48160 affected inflammatory reactions. Inflammation-related pathways (neutrophil extracellular trap formation, Th17 cell differentiation and Th1 and Th2 differentiation) were enriched in the KEGG pathway enrichment results (Figure 7C), and NSC48160 therapy significantly downregulated these pathways in comparison to the control. After NSC48160 administration, the mRNA levels of proinflammatory cytokines (Il6, Il1β, and Tnfα) and chemokines (Ccl2) were clearly lowered (Figure 7D). Meanwhile, the mRNA levels of lipid metabolism-related genes (SCD1, CPT1A, ACACA, and FASN) were regulated to the control level by NSC48160 (Figure 7D). NSC48160 inhibits the activation of the NF-κB signaling pathway which is a typical inflammatory signaling mechanism. In line with this, the protein levels of phosphorylated IKKβ and p65 were decreased in HFD-induced mice and PO-stimulated hepatocytes (Figures 7E and 7F). These findings show that NSC48160 promotes lipid metabolic processes and shields hepatocytes from inflammation and malfunction.

DISCUSSION

Due to the increasing prevalence of NAFLD/NASH and the concurrent development of HCC, preventive and curative therapy is widely desired.[20] A growing body of research highlights potential negative effects of lipid consumption, lipogenesis, and lipolysis, which are primarily triggered by abnormalities in lipid metabolism and aid in the emergence of NAFLD.[21] Therefore, the prevention and restoration of the

metabolic rewiring associated with NAFLD represent novel attractive strategies. Herein, we found the pleiotropic effects of NSC48160 on multiple processes related to oxidative stress, mitochondrial injury and inflammation through activating AMPKα signaling. AMPK plays an important role as a hub to control cell metabolism and regulate the activities of living organisms. AMPK is required for amelioration of ectopic lipid accumulation,[22] so AMPK is a vital target that we focused on in this study.

The role of AMPK in lipid metabolism has been extensively studied.[23] AMPK functions by interfering with both lipogenesis and lipid oxidation. Once activated, AMPK can phosphorylate and inactivate ACC, which leads to the failure of acetyl-CoA conversion to malonyl-CoA for fatty acid synthesis and consequently inhibits lipid accumulation in the liver.[24] Moreover, the decrease in malonyl-CoA induced by AMPK activation promotes lipid oxidation not only by increasing protein expression but also by disinhibiting the enzymatic activity of CPT1A, a rate-limiting enzyme in mitochondrial FAO.[25] In addition to ACC, AMPK activation was also reported to suppress lipogenesis by activating the SREBP-1c/FASN signaling pathway or directly phosphorylating PPARα.[26] To test our hypothesis, AMPK was silenced, via knockdown of AMPK in hepatocytes. We collected the samples and used the same method as described previously to conduct various tests and analyses. As expected, AMPK expression exhibited a close relationship with lipid metabolism. Low levels of AMPK led to aggravate HFD- or PO-induced hepatocyte injury, which was relieved by AMPK activation.

Mitochondrial metabolism sits on the crossroads of steatosis, oxidative stress and the dysregulation of metabolic pathways,[27] but its role in the pathogenesis of NAFLD has yet to be thoroughly investigated. The pathophysiology of NAFLD is connected with disrupted lipid homeostasis, which may develop into a more severe phenotype when combined with other imbalanced processes, such as increased OXPHOS, mitochondrial dysfunction, or autophagic obstruction.[28] In fact, peroxisomes are also crucial organelles that contribute to ROS generation through β-oxidation while other cellular oxidases can also generate H_2O_2.[29] NSC48160 boosted the endogenous antioxidant defense system, especially GSH, NAD^+/NADH, and peroxisomal catalase, even in the absence of aberrant mitochondrial H_2O_2. Moreover, NSC48160 treatment significantly attenuated the cellular increase in ROS/mtROS production and restored the levels of MMP. Our data indicate that the AMPKα-ACC-PPARα axis regulates these processes. PPARα controls peroxisomes β-oxidation, mitochondrial β-oxidation, fatty acid transport, mitochondrial redox status, and lipid homeostasis in the liver. The effect on the AMPKα-ACC-PPARα axis increased the antioxidant capacity of NSC48160-treated cells. The depletion of NAD^+ and GSH was found in hepatocyte with high hepatic steatosis. GSH must be synthesized within the liver either *de novo* or by the salvation pathway. Supplementation with NAD^+ and GSH may increase the amount of fat oxidized in the liver, lower oxidative stress resulting from high fat oxidation, lower the level of HS, and eventually improve liver function. In addition, it has been shown that supplementation of natural NAD^+ precursors, such as tryptophan, niacin, and nicotinamide elevates NAD^+ levels *in vivo*.[30] There is growing evidence that substantial NAD^+ synthesis may be beneficial for enhancing mitochondrial function.[31] Overall, we therefore suggest that NSC48160 increases the GSH level to normal levels, promotes the generation of NAD^+ precursors and increases the level of NAD^+ required for increased fat oxidation.

It is thought that NAFLD etiology is a complicated process. The typical damage-associated alterations found in the NAFLD model, such as inflammation and cell death, are induced by lipotoxicity.[32] Inflammation is one of the hallmarks of lipid toxicity in the liver. IKKβ and p65 secreted by injured hepatocytes are implicated in the inflammatory response generated by lipids. NSC48160 reversed inflammation in the pathological processes of NAFLD in both *in vivo* and *in vitro* models by decreasing the expression of IKKβ and p65. Furthermore, the RNA-seq results supported the potent action of NSC48160 on the inflammatory response. One notion of lipid toxicity is that apoptosis abduction, which is highly associated with the aberrant expression of apoptosis, contributes to the advancement of NAFLD.[33] Bax and caspase 9 expression levels were inhibited and we discovered that NSC48160 reduced the incidence of apoptosis in NAFLD. Taken together, NSC48160 reduced the liver damage caused by lipid toxicity in NAFLD.

In summary, the present study uncovers a mechanism underlying AMPKα activation in the presence of the small molecule NSC48160 during the therapeutic process of NASH in NAFLD. We discovered that NSC48160 significantly decreases lipid accumulation, oxidative stress and the inflammatory response by SREBP-1c mediated lipogenesis and ACC-mediated lipid metabolism as a robust inhibitor of NAFLD. Our study reveals a promising avenue for the development of a new therapy for NAFLD.

Limitations of the study

Several limitations need to be taken into consideration when interpreting the results from this study. First, lack of metabolomics data from the liver biopsy samples of clinical cases. Second, AMPK is also expressed in other tissues such as brain (hypothalamus), internal organs, adipose tissue and muscle, and thus our study exclusively focusing changes on hepatic AMPK expression may have overlooked the contribution of AMPK in other tissues to the improvement of hepatic steatosis. In the future, we will further explore the role of AMPK in the metabolism of adipose tissue by constructing specific AMPK knockout mice.

STAR★METHODS

Detailed methods are provided in the online version of this paper and include the following:

- KEY RESOURCES TABLE
- RESOURCE AVAILABILITY
  - Lead contact
  - Materials availability
  - Data and code availability

SUPPLEMENTAL INFORMATION

Supplemental information can be found online at https://doi.org/10.1016/j.isci.2023.108614.

ACKNOWLEDGMENTS

Z.J.L. and J.X.Z. thank the support from the Science and Technology Development Plan of Jilin Province (20230101145JC), National Natural Science Foundation of China (21721003), the Ministry of Science and Technology of the People's Republic of China (2016YFA0203200), the Scientific Instrument Developing Project of the Chinese Academy of Sciences (YJKYYQ20180038).

AUTHOR CONTRIBUTIONS

Z.J.L., J.X.Z., and J.W. conceived the study and participated in the overall design. J.X.Z. and X.Z.Y. performed the molecular and cellular experiments. J.X.Z. participated in the preparation and analysis of clinical subjects. J.X.Z. constructed the animal models. J.X.Z. and Z.J.L. wrote the manuscript. E.K.W. and J.W. revised the paper and participated in supervision and coordination of the study. All authors approved this manuscript for submission. All data were generated in-house, and no paper mill was used. All authors agree to be accountable for all aspects of work ensuring integrity and accuracy.

DECLARATION OF INTERESTS

The authors declare no competing interests.

INCLUSION AND DIVERSITY

We support inclusive, diverse, and equitable conduct of research.

Received: August 14, 2023
Revised: October 6, 2023
Accepted: November 29, 2023
Published: December 2, 2023

REFERENCES

1. Rom, O., Liu, Y.H., Liu, Z.P., Zhao, Y., and Wu, J.F. (2020). Glycine-based treatment ameliorates NAFLD by modulating fatty acid oxidation, glutathione synthesis, and the gut microbiome. Sci. Transl. Med. *12*, eaaz2841.
2. Wan, J., Zhang, Y.Y., Yang, D.Q., Liang, Y.J., Yang, L., Hu, S., Liu, Z., Fang, Q., Tian, S., and Ding, Y. (2021). Gastrodin improves nonalcoholic fatty liver disease via activation of the AMPK signaling pathway. Hepatology *74*, 3074–3090.
3. Zhou, F., Zhou, J., Wang, W., Zhang, X.J., Ji, Y.X., Zhang, P., She, Z.G., Zhu, L., Cai, J., and Li, H. (2019). Unexpected rapid increase in the Burden of NAFLD in China From 2008 to 2018: A systematic review and meta-analysis. Hepatology *70*, 1119–1133.
4. Min, H.K., Kapoor, A., Fuchs, M., Mirshahi, F., Zhou, H., Maher, J., Kellum, J., Warnick, R., Contos, M.J., and Sanyal, A.J. (2012). Increased hepatic synthesis and dysregulation of cholesterol metabolism is associated with the severity of nonalcoholic

fatty liver disease. Cell Metabol. *15*, 665–674.
5. Cohen, J.C., Horton, J.D., and Hobbs, H.H. (2011). Human fatty liver disease: old questions and new insights. Science *332*, 1519–1523.
6. Garcia, D., and Shaw, R.J. (2017). AMPK: Mechanisms of Cellular Energy Sensing and Restoration of Metabolic Balance. Mol. Cell *66*, 789–800.
7. Hardie, D.G. (2013). AMPK: a target for drugs and natural products with effects on both diabetes and cancer. Diabetes *62*, 2164–2172.
8. Ford, R.J., Fullerton, M.D., Pinkosky, S.L., Day, E.A., Scott, J.W., Oakhill, J.S., Bujak, A.L., Smith, B.K., Crane, J.D., Blümer, R.M., et al. (2015). Metformin and salicylate synergistically activate liver AMPK, inhibit lipogenesis and improve insulin sensitivity. Biochem. J. *468*, 125–132.
9. Zhang, J., Zhang, W., Yang, L., Zhao, W., Liu, Z., Wang, E., and Wang, J. (2023). Phytochemical gallic acid alleviates nonalcoholic fatty liver disease via AMPK-ACC-PPARα axis through dual regulation of lipid metabolism and mitochondrial function. Phytomedicine *109*, 154589.
10. Zhao, P., Sun, X., Chaggan, C., Liao, Z., In Wong, K., He, F., Singh, S., Loomba, R., Karin, M., Witztum, J.L., and Saltiel, A.R. (2020). An AMPK-caspase-6 axis controls liver damage in nonalcoholic steatohepatitis. Science *367*, 652–660.
11. Chen, Y., He, X., Chen, X., Li, Y., and Ke, Y. (2021). SeP is elevated in NAFLD and participates in NAFLD pathogenesis through AMPK/ACC pathway. J. Cell. Physiol. *236*, 3800–3807.
12. Tian, M., Hao, F., Jin, X., Sun, X., Jiang, Y., Wang, Y., Li, D., Chang, T., Zou, Y., Peng, P., et al. (2021). ACLY ubiquitination by CUL3-KLHL25 induces the reprogramming of fatty acid metabolism to facilitate iTreg differentiation. Elife *10*, e62394.
13. Li, Y., Xu, S., Mihaylova, M.M., Zheng, B., Hou, X., Jiang, B., Park, O., Luo, Z., Lefai, E., Shyy, J.Y.J., et al. (2011). AMPK phosphorylates and inhibits SREBP activity to attenuate hepatic steatosis and atherosclerosis in diet-induced insulin-resistant mice. Cell Metabol. *13*, 376–388.
14. Hu, Y., He, W., Huang, Y., Xiang, H., Guo, J., Che, Y., Cheng, X., Hu, F., Hu, M., Ma, T., et al. (2021). Fatty Acid Synthase-suppressor screening identifies sorting Nexin 8 as a therapeutic target for NAFLD. Hepatology *74*, 2508–2525.
15. Leprivier, G., Remke, M., Rotblat, B., Dubuc, A., Mateo, A.R.F., Kool, M., Agnihotri, S., El-Naggar, A., Yu, B., Somasekharan, S.P., et al. (2013). The eEF2 kinase confers resistance to nutrient deprivation by blocking translation elongation. Cell *153*, 1064–1079.
16. Faller, W.J., Jackson, T.J., Knight, J.R., Ridgway, R.A., Jamieson, T., Karim, S.A., Jones, C., Radulescu, S., Huels, D.J., Myant, K.B., et al. (2015). mTORC1-mediated translational elongation limits intestinal tumour initiation and growth. Nature *517*, 497–500.
17. Moon, Y.A., Liang, G., Xie, X., Frank-Kamenetsky, M., Fitzgerald, K., Koteliansky, V., Brown, M.S., Goldstein, J.L., and Horton, J.D. (2012). The Scap/SREBP pathway is essential for developing diabetic fatty liver and carbohydrate-induced hypertriglyceridemia in animals. Cell Metabol. *15*, 240–246.
18. Kim, J.Y., Garcia-Carbonell, R., Yamachika, S., Zhao, P., Dhar, D., Loomba, R., Kaufman, R.J., Saltiel, A.R., and Karin, M. (2018). ER stress drives lipogenesis and steatohepatitis via Caspase-2 activation of S1P. Cell *175*, 133–145.e15.
19. Covarrubias, A.J., Perrone, R., Grozio, A., and Verdin, E. (2021). NAD^+ metabolism and its roles in cellular processes during ageing. Nat. Rev. Mol. Cell Biol. *22*, 119–141.
20. Wang, H., Zhou, Y., Xu, H., Wang, X., Zhang, Y., Shang, R., O'Farrell, M., Roessler, S., Sticht, C., Stahl, A., et al. (2022). Therapeutic efficacy of FASN inhibition in preclinical models of HCC. Hepatology *76*, 951–966.
21. Pérez-Torres, I., Gutiérrez-Alvarez, Y., Guarner-Lans, V., Díaz-Díaz, E., Manzano Pech, L., and Caballero-Chacón, S.D.C. (2019). Intra-abdominal fat adipocyte hypertrophy through a progressive alteration of lipolysis and lipogenesis in metabolic syndrome Rats. Nutrients *11*, 1529.
22. Xie, L., Yuan, Y., Xu, S., Lu, S., Gu, J., Wang, Y., Wang, Y., Zhang, X., Chen, S., Li, J., et al. (2022). Downregulation of hepatic ceruloplasmin ameliorates NAFLD via SCO1-AMPK-LKB1 complex. Cell Rep. *41*, 111498.
23. Li, H., Dun, Y., Zhang, W., You, B., Liu, Y., Fu, S., Qiu, L., Cheng, J., Ripley-Gonzalez, J.W., and Liu, S. (2021). Exercise improves lipid droplet metabolism disorder through activation of AMPK-mediated lipophagy in NAFLD. Life Sci. *273*, 119314.
24. Fullerton, M.D., Galic, S., Marcinko, K., Sikkema, S., Pulinilkunnil, T., Chen, Z.P., O'Neill, H.M., Ford, R.J., Palanivel, R., O'Brien, M., et al. (2013). Single phosphorylation sites in Acc1 and Acc2 regulate lipid homeostasis and the insulin-sensitizing effects of metformin. Nat. Med. *19*, 1649–1654.
25. Sun, W., Nie, T., Li, K., Wu, W., Long, Q., Feng, T., Mao, L., Gao, Y., and Liu, Q. (2021). Hepatic CPT1A Facilitates Liver-Adipose Cross-Talk via Induction of FGF21 in Mice. Diabetes, 71:1827.
26. Zhao, Y., Yan, L., Peng, L., Huang, X., Zhang, G., Chen, B., Ren, J., Zhou, Y., Yang, L., Peng, L., et al. (2018). Oleoylethanolamide alleviates macrophage formation via AMPK/PPARα/STAT3 pathway. Pharmacol. Rep. *70*, 1185–1194.
27. Barbier-Torres, L., Fortner, K.A., Iruzubieta, P., Delgado, T.C., Giddings, E., Chen, Y., Champagne, D., Fernández-Ramos, D., Mestre, D., Gomez-Santos, B., et al. (2020). Silencing hepatic MCJ attenuates non-alcoholic fatty liver disease (NAFLD) by increasing mitochondrial fatty acid oxidation. Nat. Commun. *11*, 3360.
28. Amorim, R., Simões, I.C.M., Teixeira, J., Cagide, F., Potes, Y., Soares, P., Carvalho, A., Tavares, L.C., Benfeito, S., Pereira, S.P., et al. (2022). Mitochondria-targeted anti-oxidant AntiOxCIN4 improved liver steatosis in western diet-fed mice by preventing lipid accumulation due to upregulation of fatty acid oxidation, quality control mechanism and antioxidant defense systems. Redox Biol. *55*, 102400.
29. Sandalio, L.M., Rodríguez-Serrano, M., Romero-Puertas, M.C., and del Río, L.A. (2013). Role of peroxisomes as a source of reactive oxygen species (ROS) signaling molecules. Subcell. Biochem. *69*, 231–255.
30. Bogan, K.L., and Brenner, C. (2008). Nicotinic acid, nicotinamide, and nicotinamideriboside: a molecular evaluation of NAD^+ precursor vitamins in human nutrition. Annu. Rev. Nutr. *28*, 115–130.
31. Katsyuba, E., Mottis, A., Zietak, M., De Franco, F., van der Velpen, V., Gariani, K., Ryu, D., Cialabrini, L., Matilainen, O., Liscio, P., et al. (2018). De novo NAD^+ synthesis enhances mitochondrial function and improves health. Nature *563*, 354–359.
32. Dong, J., Viswanathan, S., Adami, E., Singh, B.K., Chothani, S.P., Ng, B., Lim, W.W., Zhou, J., Tripathi, M., Ko, N.S.J., et al. (2021). Hepatocyte-specific IL11 cis-signaling drives lipotoxicity and underlies the transition from NAFLD to NASH. Nat. Commun. *12*, 66.
33. Nasiri-Ansari, N., Nikolopoulou, C., Papoutsi, K., Kyrou, I., Mantzoros, C.S., Kyriakopoulos, G., Chatzigeorgiou, A., Kalotychou, V., Randeva, M.S., Chatha, K., et al. (2021). Empagliflozin attenuates non-alcoholic fatty liver disease (NAFLD) in high fat diet fed $ApoE^{(-/-)}$ mice by activating autophagy and reducing ER stress and apoptosi. Int. J. Mol. Sci. *22*, 818.

STAR★METHODS

KEY RESOURCES TABLE

REAGENT or RESOURCE	SOURCE	IDENTIFIER
Antibodies		
Rabbit p-AMPK	Abcam	Cat#ab133448;RRID:AB_2923300
Rabbit AMPK	Abcam	Cat#ab32047;RRID:AB_722764
Rabbit PPARα	Abcam	Cat#ab61182; RRID:AB_944764
Rabbit FAS	Abcam	Cat#ab133619 RRID:AB_2940837
Mouse SREBP-1C	Abcam	Cat#ab28481 RRID:AB_778069
Rabbit p-ACC	Abcam	Cat#ab68191 RRID:AB_11156104
Rabbit ACC	Abcam	Cat#ab45174 RRID:AB_867475
Rabbit CPT1	Abcam	Cat#ab220789 RRID:AB_2847832
Mouse β-actin	Abcam	Cat#ab8226 RRID:AB_306371
Rabbit CPS1	Abcam	Cat#ab129076 RRID:AB_11156290
Rabbit LDH	Abcam	Cat#ab53292 RRID:AB_2234531
Rabbit PDH	Abcam	Cat#ab155996 RRID:AB_2814826
Rabbit PDK1	Abcam	Cat#ab110335 RRID:AB_10858735
Rabbit PPARγ	Abcam	Cat#ab209350 RRID:AB_2890099
Rabbit IKKβ	Abcam	Cat#ab124957 RRID:AB_10975710
Rabbit p-IKKβ	Abcam	Cat#ab38515 RRID:AB_881450
Rabbit P65	Abcam	Cat#ab32536 RRID:AB_776751
Rabbit p-p65	Abcam	Cat#ab76302 RRID:AB_1524028
Biological samples		
High-fat diet, Teklad 45kcal% fat	Jinpan. Co. Ltd, China	TD.06303
Critical commercial assays		
CCK8 kit	Dojindo	CK04
BCA Protein Assay kit	Beyotime	P0011
XF Cell Mito stress test kits	Agilent Technologies	103010-100
glycolysis stress test kits	Agilent Technologies	103020-100
MMP Assay kit	Beyotime	C1071S
LDH Analysis Kit	Thermo Scientific Inc., USA	C20301

(*Continued on next page*)

Continued

REAGENT or RESOURCE	SOURCE	IDENTIFIER
Total cholesterol Assay Kit	Nanjing jiancheng Bioengineering institute	A111-1-1
Triglyceride assay kit	Nanjing jiancheng Bioengineering institute	A110-1-1
High-density lipoprotein cholesterol assay kit	Nanjing jiancheng Bioengineering institute	A112-1-1
Low-density lipoprotein cholesterol assay kit	Nanjing jiancheng Bioengineering institute	A113-1-1
Aspartate aminotransferase Assay Kit	Nanjing jiancheng Bioengineering institute	C010-2-1
Alanine aminotransferase Assay Kit	Nanjing jiancheng Bioengineering institute	C009-2-1
Deposited data		
AMPK structure	This paper	PDB:6C9H
Resequencing data	This study, NCBI Sequence Read Archive (SRA) database	PRJNA1035544
Experimental models: Cell lines		
HepG2	National of Authenticated Cell Culture	https://pubmed.ncbi.nlm.nih.gov/35931467/
BEL-7402	National of Authenticated Cell Culture	https://pubmed.ncbi.nlm.nih.gov/24219083/
Experimental models: Organisms/strains		
Mouse:Wild-type male C57BL/6N	Vital River Laboratory Animal Technology Co., Ltd	N/A
Oligonucleotides		
siRNA targeting sequence: AMPK alpha #1: GTGGAACCCTTCCATTTGA	RiboBio Technologies	N/A
Primer sequences for RT-qPCR	Table S1	N/A
Software and algorithms		
ImageJ	Faller et al.[16]	N/A
SPSS software	IBM	N/A
Metabolic network visualization	Cytoscape	https://cytoscape.org/

RESOURCE AVAILABILITY

Lead contact

Further information and requests for resources and reagents should be directed to and will be fulfilled by the lead contact, Dr. Zuojia Liu (zjliu@ciac.ac.cn).

Materials availability

This study did not generate new materials.

Data and code availability

All data reported in this paper will be shared by the lead contact upon request.
This paper does not report original code.
Any additional information required to reanalyze the data reported in this paper is available from the lead contact upon request.

EXPERIMENTAL MODEL AND SUBJECT DETAILS

Ethics statement

The animal study was reviewed and approved by the Animal Care and Use Committee of Wish Detection Technology Co., Ltd., Changchun, China (Approval Number: 20200417-1, Changchun, China).

Mouse models

C57BL/6J mice (8-week-old, male) were obtained from Beijing Vital River Laboratory Animal Technology Co., Ltd (Beijing, China). Animals were divided into three groups (n=8 per group) as follows: NCD group, HFD diet group, HFD with 50 mg/kg NSC48160 group (HFD-50) and HFD with 100 mg/kg NSC48160 group (HFD-100). Mice were provided with either a normal chow diet or a HFD diet for 16 weeks. NSC48160 was given by intraperitoneal injection every other day. During the feeding period, the fasting body weight was measured at different time points. All experimental procedures were approved by the Animal Care and Use Committee of Wish Detection Technology Co., Ltd, Changchun, China (Approval Number: SYXK 2019-0007, Changchun, China) and performed in strict accordance with Legislation Regarding the Use and Care of Laboratory Animals of China.

METHOD DETAILS

Cell culture

Cell lines (HepG2 and BEL-7402) were provided by the Chinese Academy of Sciences Cell Bank. After reaching 80% confluence, the HepG2 and BEL-7402 cells were induced of the steatosis cells with PO (OA:PA=2:1) with BSA. NSC48160 was added to the PO-BSA complex and incubated for 24 h.

Quantitative PCR assay

Total RNA was extracted from hepatocyte with Tirzol Reagent which was subsequently reverse transcribed into cDNA in accordance with the instructions. According to the manual, Real-time qPCR was performed by using SYBR Green PCR Master Mix. The relative mRNA levels of the genes' relative expression in relation to the housekeeping gene (β-actin) were calculated and expressed in comparison to the internal control. Table S1 contains the primer pairings that were utilized.

RNA sequencing and bioinformatic analysis

After being extracted, the total RNA was utilized to build the cDNA libraries. With the help of the Illumina Novaseq 6000, PE150 libraries were sequenced. The basic analysis included raw data filtering and quality control, reference genome comparison, saturation analysis, differential gene analysis, and sample correlation analysis. The usage of sophisticated analysis methods included GO/pathway/disease enrichment, differential gene coexpression network analysis, and differential gene protein interaction analysis. RNA-seq was performed by Metware Technology (Wuhan, China)

Metabolomics analysis

The total lipids were extracted from the liver in the HFD and HFD-NSC48160 groups (n=8). Liver tissues (50±2 mg) were homogenized in 1 mL mixture (include methanol and internal standard mixture). After homogenization, the mixture was vortexed and then centrifuged for 10 min at 4°C. Let the supernatant stand at -20°C for overnight. Then, the supernatant was centrifuged again for 3 min at 4°C. Finally, the supernatant was collected for liquid chromatography tandem mass spectrometry (LC-MS/MS) analysis with a QTRAP System (SCIEX, Framingham, USA). Metabonomics was performed by Metware Technology (Wuhan, China)

Surface plasmon resonance (SPR)

We conducted the experiment in accordance with the Reichert SR7500DC SPR system instructions (Reichert, New York, USA). The AMPKα protein was diluted to a final concentration of 100 μM in sodium acetate before being immobilized on a sensor chip. Additionally, it was injected via the channel. After that, channels were filled with 1 M ethanolamine, pH 8.5, to cap the chip's surface. By infusing various concentrations of the drug (1% DMSO) into AMPKα immobilized chambers (1-128 μM), the AMPKα binding affinity with NSC48160 was ascertained. TraceDrawer software was used to examine the outcomes (Reichert, New York, USA).

Cellular thermal shift assay (CETSA)

Direct binding between NSC48160 and AMPKα was found using CETSA. HCC cells were exposed to DMSO, PO or PO+NSC48160 (36 μM) for 24h. The harvested cells were gently rinsed in a pre-chilled PBS solution that contained a protease inhibitor. The samples were then heated for 3 minutes in a heat block at a range of temperatures (47°C, 49°C, 51°C, 53°C, 55°C, 57°C, 59°C, 61°C, 63°C). Proteins were isolated and Western blots were used to analyze them.

Molecular docking analysis

The RCSB Protein Data Bank provided the amino acid sequences for the carbohydrate-binding modules and the crystal structure information for AMPK (α1β1: 6C9H). Pymol V2.5.2 provides the program for processing and visualizing proteins. The protein backbone is depicted as a cartoon, with the various subunits colored in various hues. Docking was carried out according to the accepted protocol.

Measurement of serum and hepatocellular biochemical index

Cell levels of TG and T-CHO were determined by enzymatic colorimetric kits by Tecan Infinite M200 Pro (Mannedorf, Switzerland). Serum of mice was obtained in a blood collection tube by centrifuging at 1000g for 10 min. Serum and hepatocellular biochemical index quantitation was performed according to the Jian Cheng assay kit manufacturer's manual. Then, the levels of serum AST, ALT, TG, T-CHO, HDL-C, and LDL-C were measured with Tecan Infinite M200 Pro.

Histological analysis

Small pieces of fresh liver were fixed immediately in 10% buffered formalin. Sections were stained with hematoxylin and eosin (H&E). Alternatively, portions of fresh liver were flash-frozen and cryostat sections were cut and prepared for staining with Oil Red O. Pathological sections were observed under Nikon eclipse Ti-S fluorescence microscope (Nikon, Tkoyo, Japan).

Cell viability assay and lactated hydrogenase (LDH) release assay

Cell death was determined by measurements of lactated hydrogenase (LDH) release and CCK8 test. The cell viability was assessed by Cell Counting Kit-8 (CCK-8) assay kit. Briefly, the cells seeded onto 96-well plates were treated by various proportion of PO as model group or various concentrations of NSC48160 as experimental groups. Each group of cells was set five alternative holes. And then the optical density (OD) at 450 nm was read with a M200 PRO NanoQuantautoreader (TECAN, Switzerland).For LDH assay, we collected the culture medium and analyzed them by LDH Analysis Kit (Thermo Scientific Inc., USA) according to the manufacturer's instructions.

Cellular oil red O staining

The cellular lipid content was determined by Oil Red O staining. Cells were washed with PBS twice and fixed in4% paraformaldehyde for 30min, and incubated with Oil Red O working solution for another 30 min at room temperature, followed by decolorization with 60% iso-propanol. After washing three times with PBS, the cells were counterstained with hematoxylin for 30s. The cells were photographed under a light microscope (NIKON Eclipse ci, Japan).

Western blot analysis

The hepatocytes and liver tissues proteins were immunelabeled with primary antibody at 4°C overnight. After washing the membranes with TBST and incubating the membranes with fluorescence-labeled secondary antibodies at room temperature, they can be visualized by using Chemiluminescent gel imaging system (DNR MicroChemi 4.2, Israel). Band densities were quantified by Image-ProPlus (version 6.0). The internal control protein β-actin's densitometric value was used to standardize the protein level.

Detection of mitochondria reactive oxygen species

In the mitochondria of living cells, MitoSOX Red reagent was oxidized by superoxide, showing red fluorescence. The Mitochondrial ROS (mtROS) levels of cells were detected by flow cytometer using MitoSOX fluorescence reagent. After 24 h of the treatment, with or without NAC (5 mM), NSC48160 was added into the wells at the indicated concentration. The cells (1×10^6 cells/mL) were trypsinized and incubated with the MitoSOX fluorescence reagent (5 μM) at 37°C for 10 min with keeping in dark place. And then the cells were washed twice with warm buffer. The fluorescence intensity of cell was analyzed by an Accuri C6 Flow Cytometer (Franklin Lakes, USA). MitoSOX fluorescence was measured at 561 nm.

XFp cell mito stress analysis

The mitochondrial respiratory capacity was determined using XF Cell Mito Stress Test Kit. Cells seeded in the XF Cell Culture Microplate were incubated for 24 h at 37°C. And then cells were treated with PO or PO and 2.5 μM NSC48160 for 24 h. The control cells were processed in parallel. Next day, cells were incubated with the base medium containing 2 mM L-glutamine, 1 mM sodium pyruvate, and 10 mM glucose for 1 hour prior to assay. The oxygen consumption rate (OCR) was measured by XFp extracellular flux analyzer (Agilent Technologies, CA, USA). Data sets were analyzed by XFp software and then the measurements were normalized.

Immunohistochemistry

Sections of formalin-fixed paraffin-embedded liver blocks from a previous study were subjected to IHC. The following primary antibodies were used: AMPK, ACC and PPARα. The sections were incubated with the antibodies at 4°C overnight and developed by DAB substrate. And then the sections were counterstained with hematoxylin. The sections were observed with a light microscope (NIKON Eclipse ci, Japan)

and images were taken at 400× magnification. The average positive staining area percentage was measured with the Image-Pro Plus 6.0 Image Analysis System.

Measurement of tissue glutathione

Using the GSSG/GSH Quantification Kit (Dojindo Laboratories, Kumamoto, Japan), total glutathione of tissue was quantified in accordance with the manufacturer's suggested procedure.

QUANTIFICATION AND STATISTICAL ANALYSIS

Data were analyzed using SPSS software (IBM SPSS Statistics, USA). Statistical analyses were performed using the Student's t test. All values are presented as the mean ± standard error of the mean (SEM). *$p < 0.05$ and **$p < 0.01$ were considered statistically significant.